THE JOURNAL OF BIOLOGICAL CHEMISTRY VOL. 292, NO. 2, pp. 477–487, January 13, 2017

Real Time, Spatial, and Temporal Mapping of the Distribution of c-di-GMP during Biofilm Development*

Received for publication, July 5, 2016, and in revised form, November 28, 2016 Published, JBC Papers in Press, November 29, 2016, DOI 10.1074/jbc.M116.746743

Harikrishnan A. S. Nair[‡§], **Saravanan Periasamy**[‡1], **Liang Yang**[‡¶], **Staffan Kjelleberg**[‡¶], **and Scott A. Rice**[‡¶2]

From the [‡]*Singapore Centre for Environmental Life Sciences Engineering,* [§]*Interdisciplinary Graduate School, and* [¶]*School of Biological Sciences, Nanyang Technological University, Singapore 637551, Singapore*

Edited by Henrik G. Dohlman

Bis-(3′-5′)-cyclic dimeric guanosine monophosphate (c-di-GMP) is a dynamic intracellular signaling molecule that plays a central role in the biofilm life cycle. Current methodologies for the quantification of c-di-GMP are typically based on chemical extraction, representing end point measurements. Chemical methodologies also fail to take into consideration the physiological heterogeneity of the biofilm and thus represent an average c-di-GMP concentration across the entire biofilm. To address these problems, a ratiometric, image-based quantification method has been developed based on expression of the green fluorescence protein (GFP) under the control of the c-di-GMP-responsive *cdrA* promoter (Rybtke, M. T., Borlee, B. R., Murakami, K., Irie, Y., Hentzer, M., Nielsen, T. E., Givskov, M., Parsek, M. R., and Tolker-Nielsen, T. (2012) *Appl. Environ. Microbiol.* 78, 5060–5069). The methodology uses the cyan fluorescent protein (CFP) as a biomass indicator and the GFP as a c-di-GMP reporter. Thus, the CFP/GFP ratio gives the effective c-di-GMP per biomass. A binary mask was applied to alleviate background fluorescence, and fluorescence was calibrated against known c-di-GMP concentrations. Using flow cells for biofilm formation, c-di-GMP showed a non-uniform distribution across the biofilm, with concentrated hot spots of c-di-GMP. Additionally, c-di-GMP was found to be localized at the outer boundary of mature colonies in contrast to a uniform distribution in early stage, small colonies. These data demonstrate the application of a method for the *in situ*, real time quantification of c-di-GMP and show that the amount of this biofilm-regulating second messenger was dynamic with time and colony size, reflecting the extent of biofilm heterogeneity in real time.

The bacterial secondary messenger c-di-GMP[3] plays a central role in cell cycle, motility, virulence, biofilm formation, and dispersal (2). Interestingly, the intracellular concentration of c-di-GMP appears to play a role in the regulation of multiple stages of the biofilm life cycle. For example, the first step of biofilm development, reversible attachment, is regulated by flagellar movement, mediated by FleQ, a transcriptional regulator of flagellar expression. Binding of c-di-GMP to FleQ results in a conformational change, leading to downstream gene activation. Other flagellar motility-associated proteins, such as YcgR and PilZ, also have c-di-GMP binding sites and function to reduce motility as c-di-GMP increases, leading to the initiation of biofilm formation in *Pseudomonas aeruginosa* (3). During biofilm maturation, bacteria produce extracellular polysaccharides and other biofilm matrix biopolymers, which are also regulated by c-di-GMP. For example, production of the polysaccharides Pel and Psl in *P. aeruginosa* is positively regulated by c-di-GMP (4). c-di-GMP is also intimately involved in regulating biofilm dispersal. It was recently shown that the dispersed cells contain low levels of c-di-GMP compared with the biofilm cells (5). This change in c-di-GMP is likely to be a consequence of the cells perceiving particular signals or cues associated with the initiation of dispersal. For example, exposure of biofilms to nitric oxide (NO)-releasing compounds causes dispersal of *P. aeruginosa* biofilms, where exposure to NO is directly linked to the induction of phosphodiesterase activity, resulting in decreased concentrations of c-di-GMP (6). Similarly, glutamate-induced dispersal, also known as nutrient-induced dispersal, has been shown to be mediated through *dipA*, a known phosphodiesterase. The response to a wide range of signals or physiological cues may in part be controlled by distinct diguanylate cyclases (DGCs) or phosphodiesterases, where *P. aeruginosa* has been shown to encode ~40 different proteins capable of modifying c-di-GMP concentrations (7).

Given that biofilms display physiological heterogeneity (8) and that c-di-GMP-modifying enzymes also respond to changes in oxygen, nutrients, and other environmental signals, it is likely that the c-di-GMP concentration may differ in distinct regions of the biofilms, where bacteria are experiencing different concentrations of nutrients or signals. However, this heterogeneity in the distribution of c-di-GMP has not been demonstrated to date. This is due in part to the fact that the current method for quantifying c-di-GMP is based on liquid chromatography-mass spectrometry (LC-MS), which requires extraction and homogenization of the biofilm. Thus, concentrations are an average of the whole biofilm and do not take into account spatial variation in the biofilm as a consequence of metabolic gradients. To address whether there are localized c-di-GMP pools in the cell, Christen *et al.* (9) constructed a fluorescence resonance energy transfer (FRET)-based biosen-

* This work was supported by the National Research Foundation and Ministry of Education Singapore under its Research Centre of Excellence Program and a Nanyang Technological University research scholarship for the years 2012–2016. This work was also supported by Australian Research Council Grant DP140102192. The authors declare that they have no conflicts of interest with the contents of this article.

[1] Present address: Rajalakshmi Engineering College, Chennai-602105, India.
[2] To whom correspondence should be addressed. E-mail: rscott@ntu.edu.sg.

[3] The abbreviations used are: c-di-GMP, bis-(3′-5′)-cyclic dimeric guanosine monophosphate; LUT, look-up table; CFP, cyan fluorescent protein; SNP, sodium nitroprusside; RFU, relative fluorescent units.

sor to monitor the c-di-GMP concentration and demonstrated the asymmetrical distribution of c-di-GMP in planktonic cells. Therefore, such reporters, which can be calibrated to the c-di-GMP concentration, can potentially be used to address the c-di-GMP concentration in different parts of the biofilm. Similarly, Rybtke *et al.* (1) constructed a reporter for c-di-GMP, where the fluorescence intensity is directly proportional to the concentration of intracellular c-di-GMP and has been used for biofilm studies.

Here, an image-based methodology has been developed to visualize and quantify c-di-GMP *in situ* in real time using the above-mentioned reporter. The methodology allows for the visualization of c-di-GMP across the biofilm during its developmental stages, and the non-destructive nature of the methodology allowed for repeated measurements of the same biofilm, enabling dynamic quantification during biofilm development. It can also provide a spatial map of c-di-GMP across the biofilm, allowing high spatial resolution. Because the methodology uses two different fluorophores, the signals for the two fluorophores can be slightly out of alignment with each other, and this property is referred to as the chromatic shift. Further, alignment of the two different wavelengths of light could be affected as they pass through the edges of the lenses rather than through the center of the lens. This can also create a distorted image and is referred to as spherical aberration. Therefore, both the chromatic shift and the spherical aberration effects need to be accounted for to focus and align the two colors appropriately.

Using this reporter, it was observed that there was a striking difference in c-di-GMP concentrations across the biofilm where some parts of microcolonies were found to have relatively high concentrations of c-di-GMP. Additionally, c-di-GMP was found to be localized in relatively high amounts at the outer boundary of mature colonies, whereas smaller, less mature colonies showed a more uniform distribution of c-di-GMP.

Results

Evaluation of Different c-di-GMP Reporter Constructs—To determine which constructs of the *cdrA*::*gfp* reporter were the most appropriate for real time quantification of c-di-GMP concentrations, each was evaluated by confocal laser scanning microscopy. Overnight planktonic cultures were imaged, and the mean intensity of the images was calculated as the total intensity of the image divided by the total cell count. The reporter carrying the plasmid P_{cdrA}::*gfp* showed the highest relative fluorescence, 0.19 ± 0.07, whereas the least fluorescence, 0.013 ± 0.006, was observed for the strain where the construct was inserted into the genome, and that used an unstable variant of the GFP protein, Tn7-MTR2 (Tn7-P_{cdrA}::*gfp* (ASV)). The *P. aeruginosa* strain carrying the plasmid-based copy of the reporter with the unstable GFP and the strain with the reporter construct with the stable GFP inserted into the genome showed similar, very low levels of fluorescence, 0.09 ± 0.04 and 0.07 ± 0.04, respectively (Fig. 1). Although the *P. aeruginosa* strain carrying the plasmid encoded reporter with the stable GFP gave the highest levels of fluorescence, it was unsuitable for the study of dynamic changes in c-di-GMP levels here because the GFP protein half-life is 26 h (10). Therefore, the strain carrying the unstable GFP based reporter on a plasmid was selected for further studies.

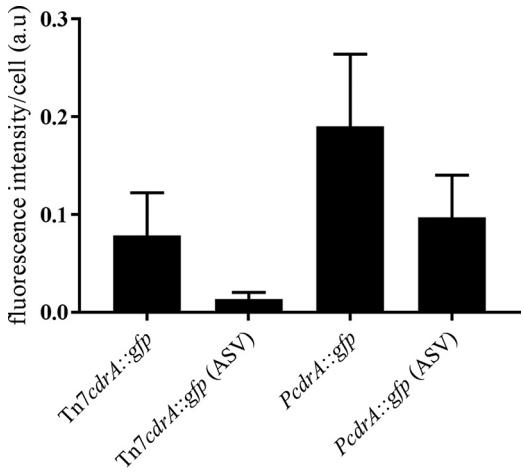

FIGURE 1. **Comparison of different *cdrA* reporter constructs in *P. aeruginosa*.** Overnight grown, planktonic cultures of *P. aeruginosa* PAO1 with different versions of the *cdrA*::*gfp* reporter construct were compared for fluorescence intensity. Reporter activity was determined based on analysis of confocal images, where the mean intensity was calculated as the total image intensity per cell. *Error bars*, S.D. ($n = 15$). *a.u.*, arbitrary units.

Plasmid Stability—Because it has been shown that the presence of antibiotics can induce biofilm formation (11) and hence may confound measures of c-di-GMP here, experiments were performed in the absence of gentamycin. *P. aeruginosa* PAO1 P_{cdrA}::*gfp* (ASV) was serially passed in conical flasks for 3 days in the presence or absence of gentamycin, at which time the cells were stained with 4′,6-diamidino-2- phenylindole (DAPI), and random images were captured using a confocal laser scanning microscope using the blue and green channels to image total cells and the c-di-GMP reporter simultaneously. The results showed that >90% of the cells maintained c-di-GMP-associated (green) fluorescence after 72 h and that there was no difference in the percentage of cells expressing GFP for the populations grown in the presence or absence of gentamicin selection (data not shown).

c-di-GMP Reporter Validation—The reporter strain has two fluorophores, where the CFP denotes the biomass and the GFP represents the c-di-GMP concentration. As noted above, it is necessary to test for and correct any chromatic aberration or shift. When fluorescent beads with similar emission spectra were tested, it was observed that there was indeed a chromatic shift in the *xz* plane but not in the *xy* plane (Fig. 2). Therefore, the *xz* shift was corrected for three-dimensional image stacks *in silico* (see "Materials and Methods").

To test the c-di-GMP reporter using planktonic cultures, where the sensitivity of the plate reader is low, the P_{cdrA}::*gfp* (ASV) reporter was transformed into a *P. aeruginosa wspF* deletion mutant. The deletion of *wspF* results in high intercellular c-di-GMP (12). However, the high c-di-GMP also results in aggregate formation, making the quantification of c-di-GMP unreliable. Therefore, the polysaccharide genes *pel* and *psl* were also deleted in the same strain, resulting in the *P. aeruginosa* mutant Δ*wspF*Δ*pslBCD*Δ*pelA*, into which the reporter P_{cdrA}::*gfp* (ASV) was introduced. Based on quantitative image

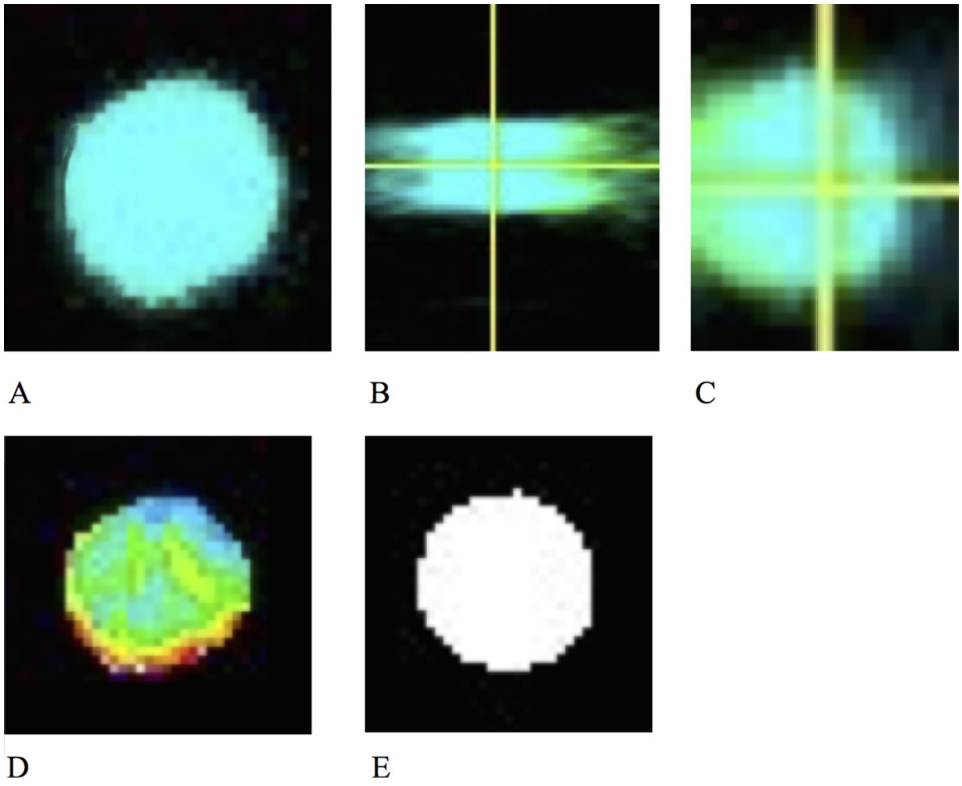

FIGURE 2. **Chromatic aberration analysis.** A 6-μm bead expressing *cyan* and *green colors* was imaged using the same imaging parameters as ratiometric imaging. *A*, the fluorescent signals in the *xy* plane showed complete overlap between *cyan* and *blue*. *B*, the chromatic aberration in the *yz* dimension was significant, showing non-overlapping *cyan* and *green* images. *C*, corrected chromatic aberration in the *yz* plane, showing overlapping *cyan* and *green images*. *D*, ratio image created with the non-corrected bead, showing intensity changes as a 16-color LUT. *E*, ratio image of the corrected bead, showing identical ratios across the entire bead. The *white color* represents a ratio of 1 in the 16-color LUT.

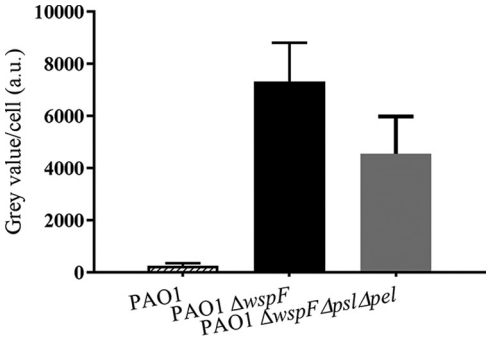

FIGURE 3. **Comparison of c-di-GMP reporter-based fluorescence of high c-di-GMP-producing mutants *versus* wild type *P. aeruginosa*.** The fluorescence intensity per cell is shown for the wild type *P. aeruginosa*, *P. aeruginosa* Δ*wspF* and *P. aeruginosa* Δ*wspF*Δ*pslBCD*Δ*pelA*. *Error bars* represent the standard deviation ($n = 3$). Magnification: 20×. *Scale bar*: 10 μm.

analysis, it was observed that the mutants *P. aeruginosa* Δ*wspF* and *P. aeruginosa* Δ*wspF*Δ*pslBCD*Δ*pelA* produced more fluorescence than the wild type *P. aeruginosa* (Fig. 3). The normalized GFP expression (and, hence, c-di-GMP concentration) was the highest for the Δ*wspF* mutant (7324.7 gray value/cell), followed by the Δ*wspF*Δ*pslBCD*Δ*pelA* mutant (4552.4 gray value/cell), and the least fluorescence was observed for the wild type *P. aeruginosa* (264.8 gray value/cell).

Dynamic Nature of the Reporter Strain—To demonstrate that the reporter produces fluorescence in proportion to c-di-GMP concentrations, treatments, such as the NO donor sodium nitroprusside (SNP), that are known to either result in decreased c-di-GMP (6) or to increase c-di-GMP (*e.g.* tellurite (TeO_2)) (13), were added to planktonic cultures, and the fluorescence responses were measured over time. The PAO1 Δ*wspF*Δ*pslBCD*Δ*pelA* mutant was used for the SNP addition studies because the baseline c-di-GMP concentration is already high, whereas the wild type strain carrying the P_{cdrA}::*gfp* (ASV) reporter was used for the c-di-GMP induction experiments using tellurite.

Fluorescence intensity can be high due to the presence of a higher number of cells; therefore, cell growth was also measured, and fluorescence was normalized to the A_{600}. Exposure of the cells to SNP resulted in an increase in growth, as measured by an increase in A_{600} (Fig. 4*A*). Exposure of bacteria (20 h) to 125 μM SNP showed the highest growth, A_{600} 1.07, followed by 250 μM SNP, reaching a maximum A_{600} of 0.91. *P. aeruginosa* PAO1 Δ*wspF*Δ*pslBCD*Δ*pelA* P_{cdrA}::*gfp* (ASV) with no added SNP only achieved a maximum A_{600} of 0.801. At the same time, exposure of *P. aeruginosa* P_{cdrA}::*gfp* (ASV) to 20 μg/ml tellurite showed reduced growth for the wild type strain, which achieved ~50% (A_{600} 0.49) of the control *P. aeruginosa* P_{cdrA}::*gfp* (ASV) within 20 h, whereas exposure to 50 μg/ml tellurite completely inhibited the growth of *P. aeruginosa* P_{cdrA}::*gfp* (ASV).

When the GFP production, an indication of the intracellular c-di-GMP concentration, was measured and normalized against growth (Fig. 4*B*), it was observed that for the NO-exposed cells, the c-di-GMP concentration was reduced in a dose-dependent manner. *P. aeruginosa* Δ*wspF*Δ*pslBCD*Δ*pelA*

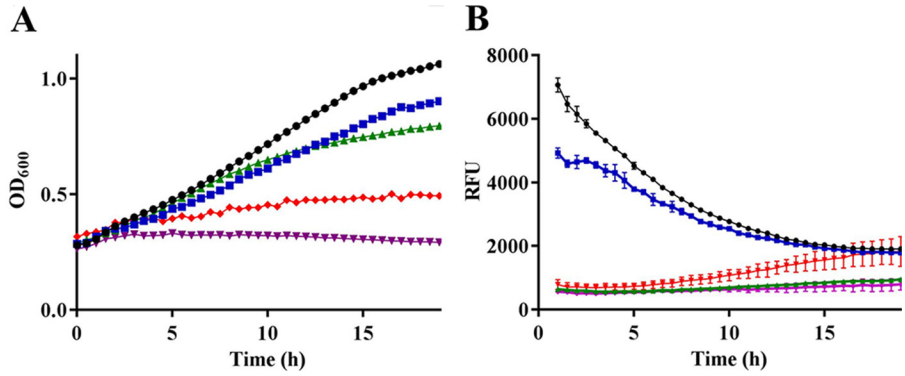

FIGURE 4. **Effect of c-di-GMP-modulating compounds on the expression of the PcdrA::*gfp* (ASV) in *P. aeruginosa*.** Bacteria were grown in 24-well plates in a Tecan plate reader with continuous shaking at 37 °C. Optical density (OD_{600}) (*A*) and fluorescence intensity (*B*) were measured every 10 min, and fluorescence intensity was normalized with the optical density and is presented as RFU. ●, *P. aeruginosa* Δ*wspF*Δ*pslBCD*Δ*pelA* P_{cdrA}::*gfp* (ASV), 125 μM SNP; ■, *P. aeruginosa* Δ*wspF*Δ*pslBCD*Δ*pelA* P_{cdrA}::*gfp* (ASV), 250 μM SNP; ▲, *P. aeruginosa* P_{cdrA}::*gfp* (ASV); ▼, *P. aeruginosa* P_{cdrA}::*gfp* (ASV), 20 μg/ml tellurite; ♦, *P. aeruginosa* P_{cdrA}::*gfp* (ASV), 50 μg/ml tellurite. Shown are representative data from three biological replicates. *Error bars*, S.D. ($n = 3$).

P_{cdrA}::*gfp* (ASV) exposed to 125 μM SNP showed a relative fluorescent intensity drop of 85% within the first 30 min. There was a 59% decrease in fluorescence for the *P. aeruginosa* Δ*wspF*Δ*pslBCD*Δ*pelA* P_{cdrA}::*gfp* (ASV) mutant in the presence of 250 μM SNP. At the same time, the wild type *P. aeruginosa* P_{cdrA}::*gfp* (ASV) with 20 μM tellurite showed a slight increase in relative fluorescence units (RFU) after 6 h of exposure, whereas no difference was observed at 50 μM tellurite. The nitric oxide donor SNP had a positive growth effect on *P. aeruginosa*, possibly due to the presence of iron, which is a part of the chemical structure of this NO donor. Although SNP exposure has been previously reported to result in decreased c-di-GMP levels (6), it is possible that the change in fluorescence of the reporter could be due to secondary effects of the treatment, as a consequence of altered growth. Therefore, careful normalization of the reporter signal against growth is necessary and ideally should include more than one measure of growth for increased confidence.

To demonstrate that the CFP signal was not affected by growth conditions, we monitored both the CFP and GFP signals separately before and after the induction of starvation conditions (Fig. 5). The raw imaging data showed that the CFP fluorescence was unchanged before and after starvation, whereas the c-di-GMP reporter fluorescence increased.

Reporter Calibration—The fluorescence response of the P_{cdrA}::*gfp* (ASV) reporter was calibrated against the intracellular concentration of c-di-GMP, as quantified by LC-MS/MS. This allows the arbitrary RFU to be correlated with cellular concentrations of c-di-GMP, and thus, the RFU can be used to estimate c-di-GMP concentration. *P. aeruginosa* P_{cdrA}::*gfp* (ASV) and *P. aeruginosa* Δ*wspF* P_{cdrA}::*gfp* (ASV) were imaged using the ratiometric imaging method described above, and subsequently the same cultures were extracted for c-di-GMP quantification using LC-MS/MS. As expected, planktonic cells of *P. aeruginosa* P_{cdrA}::*gfp* (ASV) (Fig. 6*A*) had the lowest c-di-GMP concentration, as measured by LC-MS/MS (17 pg of c-di-GMP/μg of protein) and the lowest average weighted pixel frequency of 157,507 (Fig. 6*E*). The planktonic culture of the *P. aeruginosa* Δ*wspF* mutant (Fig. 6*B*) had a higher c-di-GMP concentration of 248 pg of c-di-GMP/μg of protein than the *P. aeruginosa* P_{cdrA}::*gfp* (ASV) biofilm, 172 pg of c-di-GMP/μg of protein. The same trend was also reflected in the pixel frequency, confirming that the ratiometric based imaging correlated with chemical measurements. Planktonic cultures of *P. aeruginosa* Δ*wspF* P_{cdrA}::*gfp* (ASV) had a pixel frequency of 450,073 compared with 226,652 for biofilms of the *P. aeruginosa* P_{cdrA}::*gfp* (ASV). The planktonic culture of the *P. aeruginosa* Δ*wspF* P_{cdrA}::*gfp* (ASV) (Fig. 6*C*) exhibited pellicle formation, and within the pellicles, there were some areas with very high or very low c-di-GMP, demonstrating a non-uniform distribution of c-di-GMP. The *P. aeruginosa* Δ*wspF* P_{cdrA}::*gfp* (ASV) mutant biofilm had the highest measured c-di-GMP (587 pg of c-di-GMP/μg of protein) and the highest average weighted pixel frequency (630,083). A standard curve was generated, where the average weighted pixel frequency was plotted against the c-di-GMP concentration (Fig. 6*F*). A color scale bar was generated from the standard graph with the highest c-di-GMP concentration of 52 ng of c-di-GMP/μg of protein represented by the white color and the lowest concentration of protein, 262 pg of c-di-GMP/μg of protein, represented by the blue color.

Distribution of c-di-GMP in a Developing Biofilm—Based on the validation studies above, the spatial distribution of c-di-GMP across the different regions of a developing biofilm, as well the relative concentration of c-di-GMP, was determined for multiple stages of biofilm development. For these experiments, a flow cell biofilm was grown in the presence of M9-glucose, *z*-stack images were taken at 24-h intervals, and ratiometric imaging was applied for each time point at multiple positions across the biofilm.

Microcolonies were found to have a uniform concentration of c-di-GMP on day 2, with an average pixel frequency of 424,138 (Fig. 7*A*), and this increased to 525,174 on day 3. The overall pixel frequency on day 4 was lower, 162,321, and, in contrast to the uniform distribution observed on day 2, the distribution of c-di-GMP on day 4 appeared to be more localized, revealing areas of high and low c-di-GMP. Large colonies (diameter >50 μm) had higher concentrations of c-di-GMP at the microcolony boundary than in the interior (Fig. 7*C*). At the same time, small colonies (<50 μm) had a uniform concentration of c-di-GMP, and there was no pattern of spatial differentiation. The c-di-GMP concentration continued to decrease to

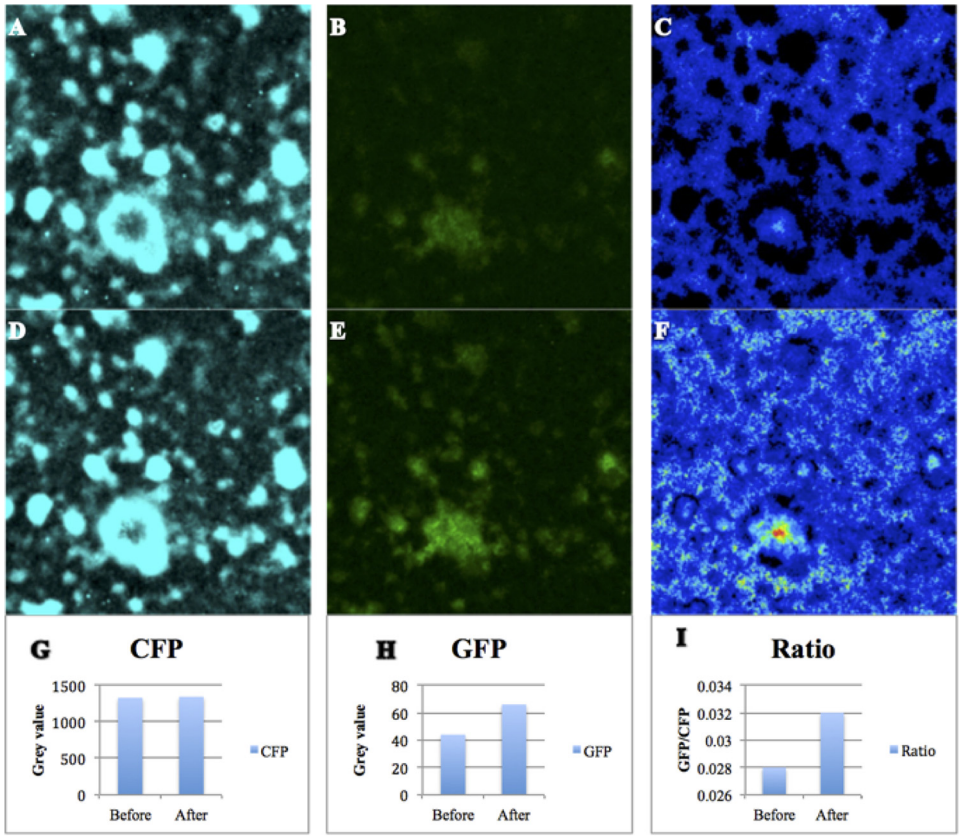

FIGURE 5. **Measurement of CFP and GFP signal separately on a *P. aeruginosa* wild type biofilm undergoing starvation.** *A–C*, before the start of carbon starvation; *D–F*, after 30 min of starvation; *G*, CFP gray values before and after treatment; *H*, GFP gray values before and after treatment; *I*, ratio of GFP/CFP before and after the induction of starvation.

day 5, reaching the lowest pixel frequency measured for the biofilm, 57,272 (Fig. 7*F*). We have previously shown that *P. aeruginosa* monoculture biofilms typically disperse at day 4 when grown in a flow cell fed with M9-glucose medium (14). Although we did not specifically quantify dispersal here, the lower level of c-di-GMP observed on day 4 was consistent with previous studies, where the biofilm typically disperses at this time point.

Discussion

The fluorescent reporter P_{cdrA}::*gfp* has been used to measure c-di-GMP in planktonic cultures (1). To use this reporter with biofilms, a ratiometric imaging method was developed here. Although ratiometric imaging is commonly used, especially for imaging intracellular levels of zinc, calcium, and pH (14, 15), it has some limitations, such as chromatic shift and spherical aberrations (16). Ratio imaging uses two different colors for imaging, with light of two different wavelengths. Chromatic aberration is the property of light to be focused at different points in space based on the wavelength. This can result in failure of the images to be superimposable despite being from the same source. This issue is generally managed through the design of corrective lenses to compensate for the chromatic shift. Both the CFP and GFP images, generated using Plan-Apochromat objectives, superimposed in the *xy*-axis almost perfectly, although there was a significant chromatic shift in the *z*-axis. Because this can give inaccurate readings for three-dimensional images, the chromatic shift was measured and corrected by adjusting the individual slices (*x-y* images) *in silico*. The ratio image of the corrected image showed perfect superimposition. In this way, all of the ratio images used in the study were corrected for the chromatic shift.

Whereas the chromatic shift can be corrected, other errors could also occur, such as spherical aberration, which is the property of light bending differentially in different parts of a lens, such as at the center or around the edges (16). This effect depends on the refractive index of the medium, thickness of the coverslip, and refractive index of the sample. Use of the correct coverslip can partly address the spherical aberration, and objective lenses are typically adjusted by the manufacturer to the correct aberration. Nonetheless, spherical aberration due to the change in refractive index remains unanswered, and there is not currently an approach to correct for this factor. For example, the fluid channels in the microcolony have a refractive index different from that of the biomass, so it is possible to have a spherical aberration when imaging the biofilm microcolony. It may be possible to directly measure these effects using an artificial biofilm made from fluorescent materials that replicates the microstructure of a biofilm as well as the fluid channels. Other factors that can impact the output or quantification based on ratiometric or other imaging techniques, including settings for laser voltage, power, gain, offset, etc., were kept constant for all imaging in this study.

The c-di-GMP reporter used here is a promoter fusion of the c-di-GMP-responsive *cdrA* gene (PA4624) with an unstable

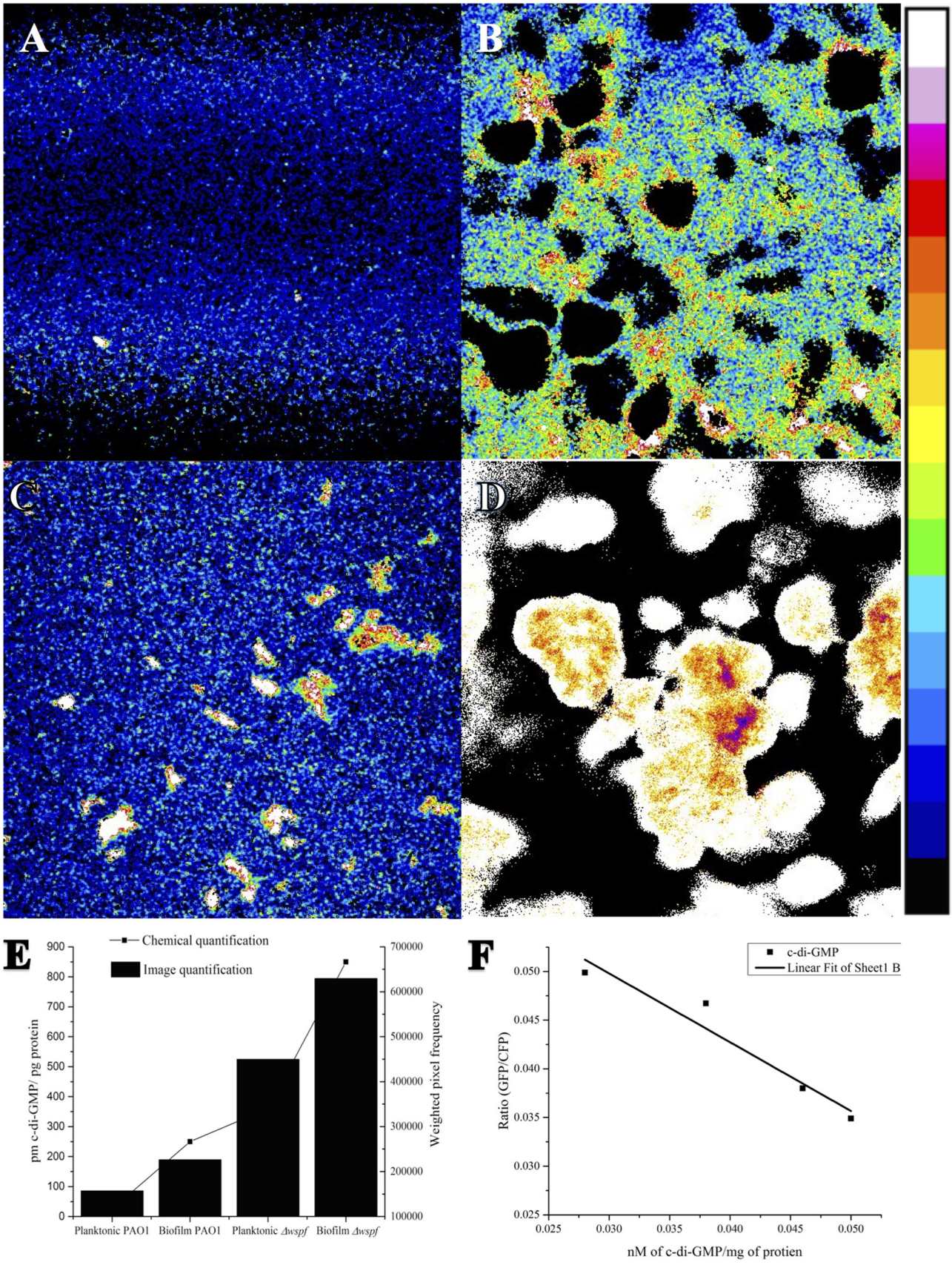

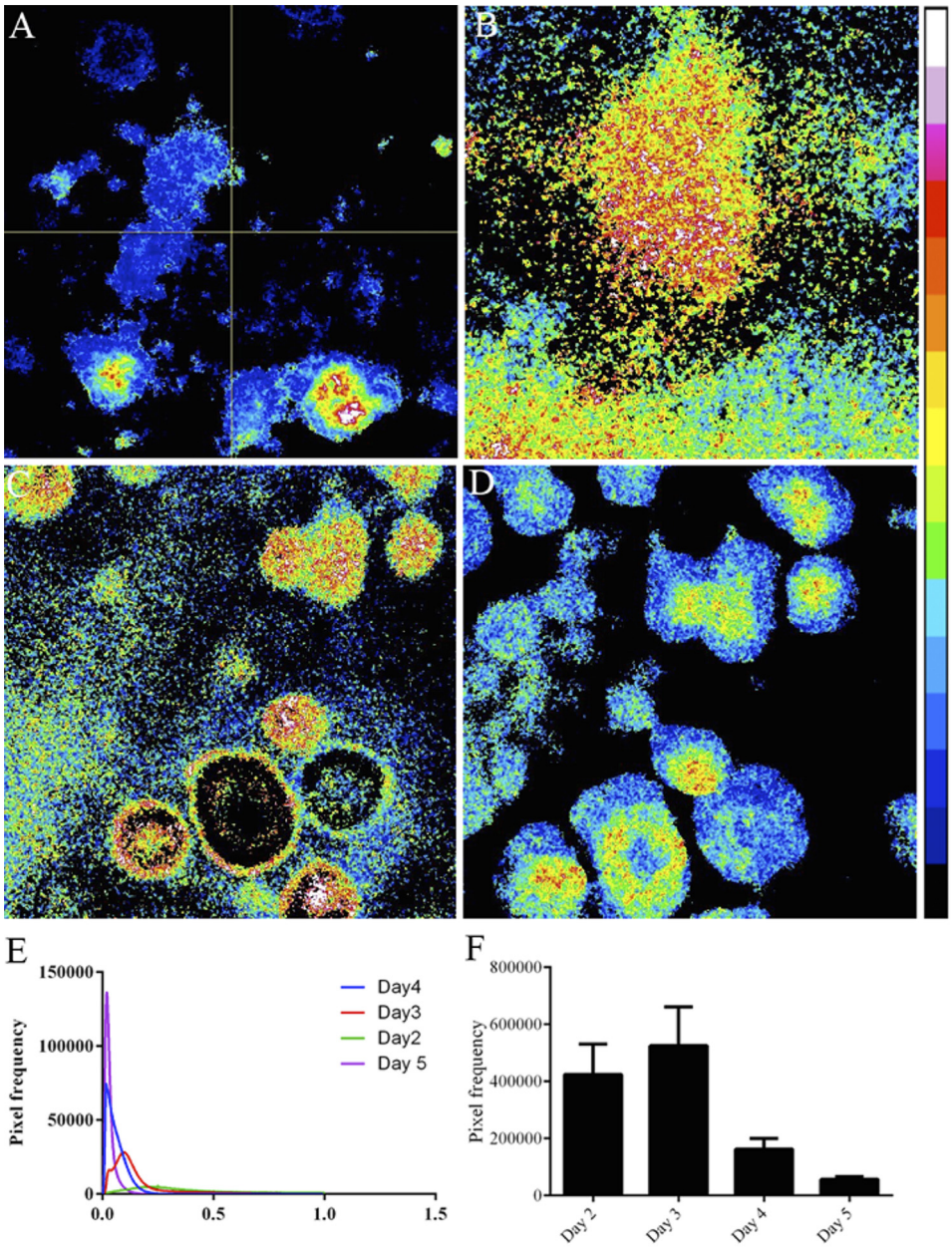

FIGURE 7. **c-di-GMP distribution across a developing *P. aeruginosa* biofilm in a flow cell.** *A*, day 2; *B*, day 3; *C*, day 4; *D*, day 5; *E*, histogram of biofilm development on days 2, 3, 4, and 5. *F*, average weighted pixel intensity as determined by the ratiometric method. The *color scale* represents the c-di-GMP concentration normalized to protein concentration, where *white* represents ~75 pM/μg protein, and *black* represents 0.38 pM/μg protein. Shown are representative data from three biological replicates. *Error bars*, S.D. ($n = 3$).

variant of the GFP (1). The mechanism of regulation of *cdrA* transcription by c-di-GMP is not known; however, the expression levels of *cdrA* strongly correlate with c-di-GMP levels. The relative levels of the *cdrA* transcript were 27-fold higher in the c-di-GMP-overproducing *wspF* strain in comparison with the wild type (17). The total c-di-GMP content of a cell includes the freely available c-di-GMP in the cell and the c-di-GMP bound to receptor proteins. However, the binding affinity of these receptor proteins is quite high (submicromolar) (18); hence, it is likely that the reporter system only responds to the free c-di-GMP in the cell.

To use the reporter system and the ratiometric imaging developed here in a semiquantitative fashion, the method was extended by binning the images into a fixed scale (Fig. 6). The

FIGURE 6. **c-di-GMP reporter PcdrA::*gfp* (ASV) calibration.** Shown are ratiometric images of planktonic *P. aeruginosa* P_{cdrA}::*gfp* (ASV) (*A*), a biofilm of *P. aeruginosa* P_{cdrA}::*gfp* (ASV) (*B*), a planktonic culture of *P. aeruginosa* Δ*wspF* P_{cdrA}::*gfp* (ASV) (*C*), and a biofilm of *P. aeruginosa* Δ*wspF* P_{cdrA}::*gfp* (ASV) (*D*). *E*, a comparison of image quantification *versus* chemical quantification. *F*, c-di-GMP concentration plotted *versus* the average weighted pixel frequency. $R^2 = 0.90827$, *x* intercept = 0.07099, *y* intercept = 0.00527, and slope = −0.70655. Magnification, ×20. The *color scale* represents the c-di-GMP concentration normalized to protein concentration in a 16-color LUT, where *white* represents ~75 pM/μg protein and *black* represents 0.38 pM/μg protein. Planktonic cultures were grown at room temperature in M9-glucose medium in a shake flask overnight, and 2 ml of culture were centrifuged in Corning® Costar® cell culture plates (24-well, flat bottom) at 811 × *g* for 10 min. Confocal images were captured after adjusting the correction ring in the ×20 lens for the thickness of the plate.

scale used here was a ratio of 0–1 in 500 bins, and this was based on comparison of multiple images from our own system. The approach also involved the implementation of a binary mask, as has been used widely in computational auditory sensing and background noise cancellation (19). The corrected masked ratio image could be used for *in situ*, non-destructive live imaging, suitable for dynamic intracellular signaling molecules, such as c-di-GMP. The ratio images for the visualization of c-di-GMP distribution in biofilm were correlated with chemical measurements of c-di-GMP. During the chemical measurement, it was observed that the triple mutant of *P. aeruginosa* Δ*wspF*Δ*pslBCD*Δ*pelA* showed less c-di-GMP than that of the *P. aeruginosa* Δ*wspF* mutant. The c-di-GMP concentration, as determined by the ratiometric method developed here, also indicated that the triple mutant had less c-di-GMP than the single mutant, although both were higher than the wild type. This may be explained by the observation that Psl can stimulate c-di-GMP production (20), and thus, the triple deletion strain would also be reduced in c-di-GMP production compared with a *wspF* strain with an intact Psl operon.

The ratio imaging of the developing biofilm showed that the distribution of c-di-GMP changed over time and had localized hot spots of high c-di-GMP across the biofilm. These areas with relatively high c-di-GMP in comparison with the neighboring areas are the first report of this kind. Similar hot spots have been observed in a variety of biological contexts, such as calcium hot spots in neuroblastoma cells and copper hot spots in vineyard soils (21, 22). The hot spots observed here could represent high c-di-GMP expression in those cells in response to local physiological conditions, or they could be the result of mutations in the bacteria in that region, leading to the constitutive overproduction of c-di-GMP. It has been shown that there is an up to 100-fold increase in the mutation rate in biofilms compared with planktonic cells (23). Such spontaneous mutations result in elevated c-di-GMP if the mutations are in genes, such as *wspF*, that are known to modify the c-di-GMP pool. Indeed, such mutants are commonly isolated from biofilms (24, 25). The non-destructive nature of the methodology allows for the repeated imaging of the same biofilm, enabling studies of the changes in c-di-GMP throughout the entire biofilm life cycle as well as in response to different treatments (*e.g.* starvation or NO treatment). Although the half-life of the unstable variant of GFP used here was 40 min (26), we saw changes in the fluorescence signal even within 10 min of the start of treatment (data not shown). Although it was not a focus of our study, we observed no evidence of photobleaching in those 10 min intervals. However, more detailed studies would be necessary to determine the limits of imaging for this reporter with regard to the bleaching phenomenon. The spatial resolution of the method developed here would be the same as for standard imaging. Because the results presented here are based on confocal microscopy, three-dimensional reconstructions of the biofilm can be generated with high spatial resolution. The resolutions in the x and y planes are on the order of several micrometers under the conditions used here, although higher magnifications or even superresolution imaging could be used to obtain higher spatial resolution.

A pattern of high c-di-GMP localized on the outside of the mature colony (diameter >50 μm) with a much lower concentration in the interior of the microcolonies was observed on day 4, whereas on days 3 and 5, the center of the biofilm was found to have high c-di-GMP. This is in agreement with the findings of Almblad *et al.* (27), where deeper layers of the biofilm have high c-di-GMP levels compared with the outside of the microcolonies after 72 h of biofilm development. The authors used the same reporter system but did not take into account the amount of biomass present, where more cells with the reporter in the same place can give rise to an apparently elevated GFP signal. To overcome this limitation, the methodology developed here normalizes the c-di-GMP signal with biomass, allowing us to continuously monitor the same biofilm. Using this approach, we have shown that the c-di-GMP pattern changes with time. This is also particularly interesting and fits with previous observations that dispersal initiates from the interior of the microcolony, where the c-di-GMP content would be expected to be lower (28), or can be observed as motile cells within the microcolony, called seething dispersal (29).

The fluorescence of GFP is dependent on oxygen, and the loss of the GFP signal observed in this study could be due to oxygen limitation in the interiors of the mature biofilm. Hansen *et al.* (30) showed that GFP fluorophore maturation can occur at levels of oxygen as low as 0.1 ppm (3.125 μM). de Beer *et al.* (31) measured the oxygen gradient in a 160-μm-thick biofilm and showed that the oxygen concentration was ~10 μM even at the substratum, which is much higher than the oxygen concentration needed for GFP to mature. Further, we and others have shown that, for constitutively expressed GFP and for the unstable GFP when used as a reporter, there is no reduction in signal, even for quite thick (60 μm) and mature biofilms (32). Nevertheless, to fully avoid the possibility of artifacts due to oxygen limitation, alternative fluorescent proteins that do not require oxygen for maturation, such as the LOV (light oxygen voltage) protein based on flavin mononucleotide (FMN) could also be used in the future (33).

Nutrient and oxygen concentrations are known to affect the c-di-GMP levels in bacteria (34). Because access to these and other nutrients by the biofilm will be dependent on a combination of diffusion and metabolic rates of the biofilm community, it is perhaps not surprising that the distribution of c-di-GMP is uneven across the biofilm. This is supported by studies using fluorescent tracers and oxygen-sensing optode that have demonstrated their heterogeneous distribution in biofilm microcolonies. In those studies, the oxygen concentrations were observed to decrease steadily from the surface of the microcolonies to the interior (35). In contrast, the amount of c-di-GMP was sharply delineated, where there was a thin, high level around the edges of the larger colonies. Thus, there did not appear to be a gradient of c-di-GMP, and further work is necessary to understand the relationship between the distribution and local oxygen or nutrient concentrations in the same regions. This difference in c-di-GMP is likely to be due to the gradients of electron donors and acceptors that are established within the biofilm, resulting in physiological stratification of the cells embedded within the matrix (8).

The distribution of c-di-GMP differed depending on microcolony size, where smaller microcolonies showed a uniform fluorescence and larger colonies only showed fluorescence around their perimeter. Because this pattern was primarily observed on day 4 at the time of dispersal, it is speculated, based on this pattern of c-di-GMP, that dispersal initiates from these larger microcolonies. This is in agreement with other studies that have indicated that after the microcolony reaches the maturation stage (~80 μm in diameter), the interior of the colony disperses from a breakout point and leaves a nonmotile, empty colony behind (36, 37). The low levels of c-di-GMP on the interior also support observations that there are often "hollow colonies" left behind after dispersal. It is proposed here that the microcolony shell is maintained by a subpopulation of cells that retain the biofilm phenotype, due to high levels of c-di-GMP, whereas the interior cells have returned to the planktonic phase.

The bacteria at the outside of the colony may experience higher nutrient and oxygen compared with the bacteria inside of the microcolonies. Thus, the application of a real time c-di-GMP reporter can provide essential information on physiological status of cells within the biofilm, which enables an improved understanding of the response of those cells to dispersal agents as well as biocides that target different populations of cells.

Materials and Methods

c-di-GMP Reporter and Transformation

Four constructs of the fluorescence-based reporter for c-di-GMP (Table 1) were obtained (1) and tested for their suitability in the current study. Electrocompetent *P. aeruginosa* PAO1 was prepared as described (38), mixed with plasmid, and electroporated (Bio-Rad Gene Pulser Xcell™ electroporation systems) using 2500 V, 25 microfarads, and 200 ohms resistance. Immediately after electroporation, 1 ml of LB broth (10 g/liter Tryptone, 5 g/liter yeast extract, and 5 g/liter NaCl) was added, and the cultures were transferred to a 15-ml tube and incubated at 37 °C for 1 h with shaking at 180 rpm. Transformants were selected by plating onto LB agar plates supplemented with 300 μg/ml carbenicillin and incubated overnight at 37 °C.

TABLE 1
c-di-GMP reporter constructs used in this study

Reporter construct	Description	Reference
Tn7 P_{cdrA}::*gfp*	Genomic insertion-stable GFP	Ref. 1
Tn7 P_{cdrA}::*gfp*(ASV)	Genomic insertion-unstable GFP	Ref. 1
P_{cdrA}::*gfp*	Plasmid-stable GFP	Ref. 1
P_{cdrA}::*gfp*(ASV)	Plasmid-unstable GFP	Ref. 1

Bacterial Strains and Culture Media

Bacteria (Table 2) were either cultured on LB agar (LB broth with 1.5% Bacto agar) or M9 minimal medium (48 mM Na_2HPO_4, 22 mM KH_2PO_4, 9 mM NaCl, 19 mM NH_4Cl, 2 mM $MgSO_4$, 0.1 mM $CaCl_2$) with 20 mM glucose.

Biofilm Development in Flow Cells

Biofilms were cultivated in three-channel flow cells (channel dimensions, 1 × 4 × 40 mm) (39). The flow cells were fed with M9 minimal medium with 20 mM glucose as a carbon source at a flow rate of 9 ml/h. Each channel was inoculated with 0.5 ml of diluted overnight culture containing ~1×10^8 cfu/ml.

c-di-GMP Measurement in Planktonic Culture

A TECAN Infinite 200 PRO plate reader was used to measure c-di-GMP in planktonic cells based on *cdrA*::*gfp* fluorescence (excitation 485 nm, emission 520 nm, excitation bandwidth 9 nm and emission bandwidth 20 nm; manual gain of 80), and growth was monitored by quantifying the absorbance at A_{600}. Measurements were recorded at 10-min intervals. The relative fluorescence, GFP/A_{600}, was calculated and was used as a measure of c-di-GMP per cell.

Microscopy and Image Analysis

Biofilm images were acquired using a Carl Zeiss confocal laser scanning microscope, CLSM 780 (Carl Zeiss, Germany), using a ×20 objective (LD plan- Neofluar ×20/0.4 Korr M27). Two separate optical channels were used to image the biofilm biomass and c-di-GMP reporter. A stably expressed CFP, inserted into the genome, was used to quantify the biomass, and GFP was quantified as a reporter for c-di-GMP. Laser voltage was measured using a Sanwa™ CD800a digital multimeter and kept at 0.587 V throughout the experiment, and pinholes of 50 and 58 μm were used for CFP and GFP, respectively. An emission bandwidth of 440–503 nm was used for CFP, and 497–598 nm was used for GFP, whereas the master gain was set to 700, and the digital gain of 1.00 was used for all of the images. Images were processed using ImageJ version 1.47 (40).

Determination of Chromatic Aberration

Blue-green fluorescent beads, 10 μm (FluoSpheres® polystyrene microspheres, Thermo Fisher Scientific) were imaged using the same parameters as above. Using the ImageJ software, a region of interest was drawn around the bead. Intensity maxima were identified by plotting the *z* axis profile for both channels individually. If the intensity maximum was on different *z* planes for the different channels, the difference is the chromatic aberration. If there was a chromatic aberration, the first few

TABLE 2
Bacterial strains used in this study

Strain	Description	Application	Reference
PAO1 Δ*wspF* P_{cdrA}::*gfp* (ASV)	Mutant expressing high c-di-GMP with c-di-GMP reporter; biofilm-forming	Positive control for biofilm studies, c-di-GMP monitoring	Ref. 1
PAO1 Δ*wspF*Δ*pslBCD*Δ*pelA* P_{cdrA}::*gfp* (ASV)	Mutant expressing high c-di-GMP with c-di-GMP reporter; non-biofilm-forming	Positive control for planktonic studies, c-di-GMP monitoring	Ref. 1
PAO1 Tn7::*gfp*	Wild type PAO1 with stable GFP	Positive control for stable GFP	This study
PAO1 P_{cdrA}::*gfp* (ASV)	Wild type PAO1 with c-di-GMP reporter	For dynamic c-di-GMP studies in planktonic cells	This study
PAO1 Tn7-Gm- eCFP P_{cdrA}::*gfp* (ASV)	Wild type PAO1 stably expressing CFP with c-di-GMP reporter	For c-di-GMP quantification in biofilm	This study

slices at one channel were duplicated and slices at the end of other channel were added to match the total number of slices. Making a composite image with this corrected image solved any chromatic aberrations.

In Situ Ratiometric Imaging

To map the spatial distribution of c-di-GMP across the biofilm, it was necessary to develop a method that would allow for normalization of the c-di-GMP-related GFP expression with the total cell numbers. Thus, *z*-stack images were captured by confocal microscopy, and the images were then separated into channels corresponding to either CFP, representing the biomass, or GFP, representing c-di-GMP. Dividing the reporter channel (GFP) by the biomass channel (CFP) gives a ratio for each image, and this ratio is presented as a pseudocolor image representing the effective amount of c-di-GMP per biomass. Areas where there is no biofilm or where there is some background fluorescence can artificially inflate the normalized data. Therefore, a mask was created from the biomass channel by adjusting the threshold. The mask was then converted to a binary format by dividing by 255 (the maximum pixel value of an 8-bit image; $2^8 - 1 = 255$). The resulting binary mask contains values of either 0 or 1, where 1 represents the biomass and 0 is the background. Multiplying the masked image with the ratio image gives the masked ratio image, eliminating background. The masked ratio image was then segmented into 500 bins from 0 to 1 to create a histogram. This histogram can be used for quantifying images or comparison of different images. The masked ratio image was then converted to a look-up table "16 colors" for visualizing the c-di-GMP distribution. The ratio of GFP/CFP of 1 was colored as white and that of 0 was set to black. Using this approach, the areas colored in red correlate with microcolonies having high c-di-GMP, whereas the yellow region represents parts of the biofilm with lower concentrations of c-di-GMP.

Chemical Quantification of c-di-GMP by LC-MS/MS

Biomass Extraction from Flow Cell Biofilms—The planktonic phase of the flow cell biofilms were carefully decanted by tilting the flow cell to one end. A syringe containing 2 ml of 1 mM ice-cold ammonium acetate was attached to one end of the flow cell, and another empty syringe was connected at the other end. The biomass inside the flow cell was removed through back and forth (10 times) washing using the syringes.

c-di-GMP Extraction—Two milliliters of planktonic culture or 1.5 ml of extracted biofilm were centrifuged (10,000 × *g* for 10 min at 4 °C), and the pellets were washed with 2 ml of ice-cold 1 mM ammonium acetate. The pellets were then resuspended in 2 ml of ice-cold acetonitrile, methanol, water (40:40:20) and homogenized by passing it five times through a 20-gauge needle. The solution was then lysed for 30 min (power 100%, frequency 37 kHz) in a water bath sonicator (Elma Schmidbauer GmbH, Singen, Germany) filled with ice water. The cell debris was then centrifuged at 10,000 × *g* for 10 min at 4 °C, and the supernatant was retained and kept on ice. The pellet was again resuspended in 2 ml of ice-cold acetonitrile, methanol, water (40:40:20), and extraction was repeated once more as above. The extracts were evaporated at 4 °C in a cooling SpeedVac (CentriVap® benchtop vacuum concentrators) coupled with a CentriVap Cold Trap (Labconco Corp., 73850 series) until the volume reached ~500 μl. The extracted mixture was then cooled to −80 °C and freeze-dried overnight (Labconco FreeZone 4.5-liter benchtop freeze dry system). The dried extract was dissolved in 200 μl of 1 mM ice-cold ammonium acetate and centrifuged at 10,000 × *g* for 10 min at 4 °C. The supernatant was then transferred to HPLC vials and analyzed by LC-MS/MS (NUS-Environmental Research Institute at the National University of Singapore).

LC-MS/MS—Quantification of c-di-GMP was performed in an EQuan MAX™ LC-MS system, using an Accela 1250 UHPLC pump connected to a Thermo Velos Pro Orbitrap mass spectrometer (Thermo Fisher Scientific). Chromatographic separation was achieved using a Nucleodur C18 pyramid column (2 × 50 mm, 3 μm) (Macherey-Nagel GmbH, Düren, Germany), held at 40 °C, with a solvent flow rate of 0.3 ml/min and an injection volume of 10 μl. The mobile phase A was 10 mM ammonium acetate buffer, containing 0.1% formic acid, and the mobile phase B was acetonitrile, containing 0.1% formic acid. The solvent gradient conditions were as follows: 0% B from 0 min to 10% at 3 min, 90% at 4 min, hold for 5 min, and then returned to 0% at 5.5 min and equilibrated for 4.5 min, with a total run time of 10 min.

Quantification was performed by positive ion electrospray ionization, using selected ion monitoring scan type with center mass *m*/*z* 691.1021 at high resolution (60,000). For qualitative analysis, MS/MS was performed using collision-induced dissociation with normalized collision energy 20 (of maximum), with an isolation width of 1 Da and activation time of 30 min. The MS conditions were as follows: source voltage 3.6 kV; heater and capillary temperature 300 °C; sheath, auxiliary, and sweeper gas flows 40, 15, and 1 (arbitrary units), respectively.

Protein Quantification—Protein concentrations were determined using the bicinchoninic acid assay (BCA) protocol, where 1 ml of planktonic culture or 500 μl of biofilm extract was pelleted by centrifugation (10,000 × *g* for 10 min at 4 °C) and washed once with PBS (137 mM NaCl, 2.7 mM KCl, 10 mM Na_2HPO_4, 2 mM KH_2PO_4). The pellets were then resuspended in 1 ml of lysis buffer (0.1% SDS, 0.5 M triethylammonium hydrogen carbonate buffer, Sigma-Aldrich) and homogenized by passing five times through a 20-gauge needle. The solution was then lysed for 30 min (power 100%, frequency 37 kHz) in a water bath sonicator filled with ice water. The extracted material was then centrifuged at 10,000 × *g* for 10 min at 4 °C. A standard curve was generated using 25 μl of BSA standards (2000 to 0 μg/ml) to quantify sample protein concentrations in triplicate at 562 nm.

Author Contributions—H. A. S. N. performed experiments along with S. P. H. A. S. N., S. K., and S. A. R. conceived and designed experiments. H. A. S. N., S. P., Y. L., S. K., and S. A. R. interpreted the data. H. A. S. N., Y. L., S. K., and S. A. R. contributed to the writing of the manuscript, and all authors approved the final version of the manuscript.

References

1. Rybtke, M. T., Borlee, B. R., Murakami, K., Irie, Y., Hentzer, M., Nielsen, T. E., Givskov, M., Parsek, M. R., and Tolker-Nielsen, T. (2012) Fluorescence-based reporter for gauging cyclic di-GMP levels in *Pseudomonas aeruginosa*. *Appl. Environ. Microbiol.* **78,** 5060–5069
2. Jenal, U., and Malone, J. (2006) Mechanisms of cyclic-di-GMP signaling in bacteria. *Annu. Rev. Genet.* **40,** 385–407
3. Baraquet, C., and Harwood, C. S. (2013) Cyclic diguanosine monophosphate represses bacterial flagella synthesis by interacting with the Walker A motif of the enhancer-binding protein FleQ. *Proc. Natl. Acad. Sci. U.S.A.* **110,** 18478–18483
4. Franklin, M. J., Nivens, D. E., Weadge, J. T., and Howell, P. L. (2011) Biosynthesis of the *Pseudomonas aeruginosa* extracellular polysaccharides, alginate, Pel, and Psl. *Front. Microbiol.* **2,** 167
5. Chua, S. L., Liu, Y., Yam, J. K. H., Chen, Y., Vejborg, R. M., Tan, B. G. C., Kjelleberg, S., Tolker-Nielsen, T., Givskov, M., and Yang, L. (2014) Dispersed cells represent a distinct stage in the transition from bacterial biofilm to planktonic lifestyles. *Nat. Commun.* **5,** 4462
6. Barraud, N., Schleheck, D., Klebensberger, J., Webb, J. S., Hassett, D. J., Rice, S. A., and Kjelleberg, S. (2009) Nitric oxide signaling in *Pseudomonas aeruginosa* biofilms mediates phosphodiesterase activity, decreased cyclic di-GMP levels, and enhanced dispersal. *J. Bacteriol.* **191,** 7333–7342
7. Römling, U., Galperin, M. Y., and Gomelsky, M. (2013) Cyclic di-GMP: the first 25 years of a universal bacterial second messenger. *Microbiol. Mol. Biol. Rev.* **77,** 1–52
8. Stewart, P. S., and Franklin, M. J. (2008) Physiological heterogeneity in biofilms. *Nat. Rev. Microbiol.* **6,** 199–210
9. Christen, M., Kulasekara, H. D., Christen, B., Kulasekara, B. R., Hoffman, L. R., and Miller, S. I. (2010) Asymmetrical distribution of the second messenger c-di-GMP upon bacterial cell division. *Science* **328,** 1295–1297
10. Corish, P., and Tyler-Smith, C. (1999) Attenuation of green fluorescent protein half-life in mammalian cells. *Protein Eng.* **12,** 1035–1040
11. Hoffman, L. R., D'Argenio, D. A., MacCoss, M. J., Zhang, Z., Jones, R. A., and Miller, S. (2005) Aminoglycoside antibiotics induce bacterial biofilm formation. *Nature* **436,** 1171–1175
12. Hickman, J. W., Tifrea, D. F., and Harwood, C. S. (2005) A chemosensory system that regulates biofilm formation through modulation of cyclic diguanylate levels. *Proc. Natl. Acad. Sci. U.S.A.* **102,** 14422–14427
13. Chua, S. L., Sivakumar, K., Rybtke, M., Yuan, M., Andersen, J. B., Nielsen, T. E., Givskov, M., Tolker-Nielsen, T., Cao, B., Kjelleberg, S., and Yang, L. (2015) C-di-GMP regulates *Pseudomonas aeruginosa* stress response to tellurite during both planktonic and biofilm modes of growth. *Sci. Rep.* **5,** 10052
14. Taki, M., Wolford, J. L., and O'Halloran, T. V. (2004) Emission ratiometric imaging of intracellular zinc: design of a benzoxazole fluorescent sensor and its application in two-photon microscopy. *J. Am. Chem. Soc.* **126,** 712–713
15. Kikuchi, K., Komatsu, K., and Nagano, T. (2004) Zinc sensing for cellular application. *Curr. Opin. Chem. Biol.* **8,** 182–191
16. North, A. J. (2006) Seeing is believing? A beginners' guide to practical pitfalls in image acquisition. *J. Cell Biol.* **172,** 9–18
17. Borlee, B. R., Goldman, A. D., Murakami, K., Samudrala, R., Wozniak, D. J., and Parsek, M. R. (2010) *Pseudomonas aeruginosa* uses a cyclic-di-GMP-regulated adhesin to reinforce the biofilm extracellular matrix. *Mol. Microbiol.* **75,** 827–842
18. Chou, S.-H., and Galperin, M. Y. (2016) Diversity of cyclic-di-GMP-binding proteins and mechanisms. *J. Bacteriol.* **198,** 32–46
19. Wang, D. (2005) On ideal binary mask as the computational goal of auditory scene analysis. in *Speech Separation by Humans and Machines*, 10th Ed. (Divenyi, P., ed) pp. 181–197, Springer, New York
20. Irie, Y., Borlee, B. R., O'Connor, J. R., Hill, P. J., Harwood, C. S., Wozniak, D. J., and Parsek, M. R. (2012) Self-produced exopolysaccharide is a signal that stimulates biofilm formation in *Pseudomonas aeruginosa*. *Proc. Natl. Acad. Sci. U.S.A.* **109,** 20632–20636
21. Silver, R. A., Lamb, A. G., and Bolsover, S. R. (1990) Calcium hotspots caused by L-channel clustering promote morphological changes in neuronal growth cones. *Nature* **343,** 751–754
22. Jacobson, A. R., Dousset, S., Andreux, F., and Baveye, P. C. (2007) Electron microprobe and synchrotron X-ray fluorescence mapping of the heterogeneous distribution of copper in high-copper vineyard soils. *Environ. Sci. Technol.* **41,** 6343–6349
23. Conibear, T. C., Collins, S. L., and Webb, J. S. (2009) Role of mutation in *Pseudomonas aeruginosa* biofilm development. *PLoS One* **4,** e6289
24. Kelvin Lee, K. W., Hoong Yam, J. K., Mukherjee, M., Periasamy, S., Steinberg, P. D., Kjelleberg, S., and Rice, S. A. (2016) Interspecific diversity reduces and functionally substitutes for intraspecific variation in biofilm communities. *ISME J.* **10,** 846–857
25. Koh, K. S., Lam, K. W., Alhede, M., Queck, S. Y., Labbate, M., Kjelleberg, S., and Rice, S. A. (2007) Phenotypic diversification and adaptation of *Serratia marcescens* MG1 biofilm-derived morphotypes. *J. Bacteriol.* **189,** 119–130
26. Andersen, J. B., Sternberg, C., Poulsen, L. K., Bjorn, S. P., Givskov, M., and Molin, S. (1998) New unstable variants of green fluorescent protein for studies of transient gene expression in bacteria. *Appl. Environ. Microbiol.* **64,** 2240–2246
27. Almblad, H., Harrison, J. J., Rybtke, M., Groizeleau, J., Givskov, M., Parsek, M. R., and Tolker-Nielsen, T. (2015) The cyclic AMP-Vfr signaling pathway in *Pseudomonas aeruginosa* is inhibited by cyclic-di-GMP. *J. Bacteriol.* **197,** 2190–2200
28. Stewart, P. S., Rani, S. A., Gjersing, E., Codd, S. L., Zheng, Z., and Pitts, B. (2007) Observations of cell cluster hollowing in *Staphylococcus epidermidis* biofilms. *Lett. Appl. Microbiol.* **44,** 454–457
29. Hunt, S. M., Werner, E. M., Huang, B., Hamilton, M. A., and Stewart, P. S. (2004) Hypothesis for the role of nutrient starvation in biofilm detachment. *Appl. Environ. Microbiol.* **70,** 7418–7425
30. Hansen, M. C., Palmer, R. J., Jr., Udsen, C., White, D. C., and Molin, S. (2001) Assessment of GFP fluorescence in cells of *Streptococcus gordonii* under conditions of low pH and low oxygen concentration. *Microbiology* **147,** 1383–1391
31. de Beer, D., Stoodley, P., Roe, F., and Lewandowski, Z. (1994) Effects of biofilm structures on oxygen distribution and mass transport. *Biotechnol. Bioeng.* **43,** 1131–1138
32. Hwang, G., Liu, Y., Kim, D., Sun, V., Aviles-Reyes, A., Kajfasz, J. K., Lemos, J. A., and Koo, H. (2016) Simultaneous spatiotemporal mapping of *in situ* pH and bacterial activity within an intact 3D microcolony structure. *Sci. Rep.* **6,** 32841
33. Drepper, T., Eggert, T., Circolone, F., Heck, A., Krauss, U., Guterl, J.-K., Wendorff, M., Losi, A., Gärtner, W., and Jaeger, K.-E. (2007) Reporter proteins for *in vivo* fluorescence without oxygen. *Nat. Biotechnol.* **25,** 443–445
34. Gjermansen, M., Ragas, P., Sternberg, C., Molin, S., and Tolker-Nielsen, T. (2005) Characterization of starvation-induced dispersion in *Pseudomonas putida* biofilms. *Environ. Microbiol.* **7,** 894–906
35. Rani, S. A., Pitts, B., and Stewart, P. S. (2005) Rapid diffusion of fluorescent tracers into *Staphylococcus epidermidis* biofilms visualized by time lapse microscopy. *Antimicrob. Agents Chemother.* **49,** 728–732
36. Purevdorj-Gage, B., Costerton, W. J., and Stoodley, P. (2005) Phenotypic differentiation and seeding dispersal in non-mucoid and mucoid *Pseudomonas aeruginosa* biofilms. *Microbiology* **151,** 1569–1576
37. Kirov, S. M., Webb, J. S., O'may, C. Y., Reid, D. W., Woo, J. K., Rice, S. A., and Kjelleberg, S. (2007) Biofilm differentiation and dispersal in mucoid *Pseudomonas aeruginosa* isolates from patients with cystic fibrosis. *Microbiology* **153,** 3264–3274
38. Choi, K.-H., and Schweizer, H. P. (2005) An improved method for rapid generation of unmarked *Pseudomonas aeruginosa* deletion mutants. *BMC Microbiol.* **5,** 30
39. Tolker-Nielsen, T., and Sternberg, C. (2011) Growing and analyzing biofilms in flow chambers. *Curr. Protoc. Microbiol.* 10.1002/9780471729259.mc01b02s21
40. Abràmoff, M. D., Magalhães, P. J., and Ram, S. J. (2004) Image processing with ImageJ. *Biophototonics Int.* **11,** 36–42

Real Time, Spatial, and Temporal Mapping of the Distribution of c-di-GMP during Biofilm Development

Harikrishnan A. S. Nair, Saravanan Periasamy, Liang Yang, Staffan Kjelleberg and Scott A. Rice

J. Biol. Chem. 2017, 292:477-487.
doi: 10.1074/jbc.M116.746743 originally published online November 29, 2016
